Measurement of the modulation transfer function of an X-ray microscope based on multiple Fourier orders analysis of a Siemens star

Joaquín Otón,[1,*] Carlos Oscar S. Sorzano,[1] Roberto Marabini,[2] Eva Pereiro[3] and Jose M. Carazo[1]

[1]*Biocomputing Unit, National Center for Biotechnology (CSIC), c/Darwin, 3, Campus Universidad Autónoma, 28049 Madrid, Spain*
[2]*Escuela Politecnica Superior, Univ. Autonoma de Madrid, Campus. Univ. Autonoma de Madrid, 28049 Cantoblanco, Madrid, Spain*
[3]*ALBA Synchrotron Light Source, 08290 Cerdanyola del Valls, Barcelona, Spain*

[*]*joton@cnb.csic.es*

http://biocomp.cnb.csic.es

Abstract: Soft X-ray tomography (SXT) is becoming a powerful imaging technique to analyze eukaryotic whole cells close to their native state. Central to the analysis of the quality of SXT 3D reconstruction is the estimation of the spatial resolution and Depth of Field of the X-ray microscope. In turn, the characterization of the Modulation Transfer Function (MTF) of the optical system is key to calculate both parameters. Consequently, in this work we introduce a fully automated technique to accurately estimate the transfer function of such an optical system. Our proposal is based on the preprocessing of the experimental images to obtain an estimate of the input pattern, followed by the analysis in Fourier space of multiple orders of a Siemens Star test sample, extending in this way its measured frequency range.

OCIS codes: (110.4850) Optical transfer functions; (110.4100) Modulation transfer function; (340.6720) Synchrotron radiation; (340.7460) X-ray microscopy; (340.7440) X-ray imaging; (260.6048) Soft x-rays.

References and links

1. R. Burge, X.-C. Yuan, G. Morrison, P. Charalambous, M. Browne, and Z. An, "Incoherent imaging with the soft X-ray microscope," Ultramicroscopy **83**, 75–92 (2000).
2. R. R. Meyer and A. I. Kirkland, "Characterisation of the signal and noise transfer of CCD cameras for electron detection," Microsc. Res. Techniq. **49**, 269–280 (2000).
3. H. Takano, S. Konishi, T. Koyama, Y. Tsusaka, S. Ichimaru, T. Ohchi, H. Takenaka, and Y. Kagoshima, "Point spread function measurement of an X-ray beam focused by a multilayer zone plate with narrow annular aperture," J. Synchrotron Radiat. **21**, 446–448 (2014).
4. S. Reichenbach, S. K. Park, and R. Narayanswamy, "Characterizing digital image acquisition devices," Opt. Eng. **30**, 170–177 (1991).
5. C. D. Claxton and R. C. Staunton, "Measurement of the point-spread function of a noisy imaging system," J. Opt. Soc. Am. A **25**, 159–170 (2008).
6. L. Chen, J. McGinty, H. B. Taylor, L. Bugeon, J. R. Lamb, M. J. Dallman, and P. M. W. French, "Incorporation of an experimentally determined MTF for spatial frequency filtering and deconvolution during optical projection tomography reconstruction," Opt. Express **20**, 7323–7337 (2012).

#227116 - $15.00 USD Received 25 Nov 2014; revised 23 Jan 2015; accepted 27 Jan 2015; published 6 Apr 2015

7. W. V. D. Broek, S. V. Aert, and D. V. Dyck, "Fully automated measurement of the modulation transfer function of charge-coupled devices above the Nyquist frequency," Microsc. Microanal. **18**, 336–342 (2012).
8. R. S. Ruskin, Z. Yu, and N. Grigorieff, "Quantitative characterization of electron detectors for transmission electron microscopy," J. Struct. Biol. **184**, 385–393 (2013).
9. P. a. C. Takman, H. Stollberg, G. A. Johansson, A. Holmberg, M. Lindblom, and H. M. Hertz, "High-resolution compact X-ray microscopy," J. Microsc. **226**, 175–181 (2007).
10. M. C. Bertilson, O. von Hofsten, M. Lindblom, T. Wilhein, H. M. Hertz, and U. Vogt, "Compact high-resolution differential interference contrast soft X-ray microscopy," Appl. Phys. Lett. **92**, 064104 (2008).
11. S. Rehbein, P. Guttmann, S. Werner, and G. Schneider, "Characterization of the resolving power and contrast transfer function of a transmission X-ray microscope with partially coherent illumination," Opt. Express **20**, 1–3 (2012).
12. D. B. Carlson, J. Gelb, V. Palshin, and J. E. Evans, "Laboratory-based cryogenic soft X-ray tomography with correlative cryo-light and electron microscopy," Microsc. Microanal. **19**, 22–29 (2013).
13. R. Reulke, S. Becker, N. Haala, and U. Tempelmann, "Determination and improvement of spatial resolution of the CCD-line-scanner system ADS40," ISPRS J. Photogramm. Remote Sens. **60**, 81–90 (2006).
14. J. W. Goodman, *Introduction to Fourier Optics* (McGraw-Hill, 1996).
15. M. Born and E. Wolf, *Principles of Optics: Electromagnetic Theory of Propagation, Interference and Diffraction of Light* (Cambridge University, 1999), 7th ed.
16. C. Chang and T. Nakamura, "Partially coherent image formation theory for X-ray microscopy," in "Microscopy: Science, Technology, Applications and Education," , M.-V. A. and D. J., eds. (Formatex Research Center, 2010), 3, pp. 1897–1904, 4th ed.
17. J. W. Goodman, *Statistical Optics* (Wiley, 2000).
18. E. Pereiro, J. Nicolás, S. Ferrer, and M. R. Howells, "A soft X-ray beamline for transmission X-ray microscopy at ALBA," J. Synchrotron Radiat. **16**, 505–512 (2009).

1. Introduction

The characterization of the key magnitudes of an optical system, such as the transfer function or the depth of field (DOF) [1], is a key process both to perform the appropriate processing on the experimental images and to, ultimately, understand the limits of the so obtained results.

Several methods to measure the MTF can be found in the literature. One of the best known techniques is the so-called knife-edge method, where a straight-edged test plate is imaged in the microscope. The measured 1D intensity profile normal to the edge is the *edge spread function* (ESF). From this profile the most common method to obtain the MTF is the analysis of the *line spread function* through the differentiation of the ESF [2, 3]. However, the use of discrete approximations of the derivative function introduces a bandpass filter, an effect that can be minimized by analyzing directly the ESF [4–6]. Moreover, the application of this approach to SXT requires the very accurate fabrication of a microscopically straight-edged test plate, a process that has not proven to be easy.

An alternative method, where the specific fabrication of a test plate is not necessary, is the one known as *beam blocker* method, where the own beam stopper of the microscope can be used [7, 8]. A good estimation of the input binary image of the blocker, used for deconvolution, can be obtained setting a threshold in the measured image, subsequently deriving the MTF as a combination of several Gaussian functions by an iterative process.

In this work we propose a method based on a new analysis of another well-known test pattern, a Siemens star (SS) (Fig. 1(a)), in which we greatly minimize any possible division by small numbers, as it may be the case in a deconvolution process, as well as avoid iterative approaches. This test pattern is characterized by an angular periodic structure where the frequency of the fringes depends on the radius. This pattern is usually analyzed along constant radial profiles to obtain the angular mean contrast value for the corresponding resolution, known as the *contrast transfer function* [9–11]. Other authors have analyzed the visibility of the fringes to establish a qualitative cut-off frequency [12]. However, the range of frequencies related to the different crowns of the SS does not directly cover all the frequential domain of the optical system of the microscope. Consequently, in this paper we introduce a new direct method to measure the MTF

#227116 - $15.00 USD Received 25 Nov 2014; revised 23 Jan 2015; accepted 27 Jan 2015; published 6 Apr 2015

by analyzing the Fourier transform of the SS angular profiles. The two key concepts supporting our approach are: (1) The experimental estimation of the input image through a preprocessing of the measured images, avoiding to consider the SS as a perfectly symmetric rectangle shaped periodic function, as in previous works [13], (2) The use of multiple Fourier orders of the Fourier transform of the SS, extending the frequential range of our estimations.

2. Modulation transfer function

In optics, the concept of *transfer function* allows for a conceptually easy way to understand the relationship between input and output in a given system, particularly important for linear systems. In fact, related to the concrete magnitude used to establish the linear relationship, we find appropriate definitions for *amplitude transfer function* for coherent systems and *optical transfer function* for totally incoherent systems, with well-known relationships between them [14]. The case of partially coherent systems is more complex. On the one hand, in this case the linearity applies to the propagation of the mutual intensity [15, 16], and it is related to the numerical aperture of both the imaging and condenser lenses. On the other hand, being the mutual intensity a 4 dimensional function, it is not possible to plot the real *transfer function* as in the case of totally incoherent/coherent illumination. Actually, what is usually considered in the literature is the *apparent transfer function* (ATF) [17], defined as

$$\mathscr{H}_A(f_x,f_y)=\frac{\tilde{I}_{out}(f_x,f_y)}{\tilde{I}_{in}(f_x,f_y)}, \tag{1}$$

where $\tilde{I}_{in}(f_x,f_y)$ and $\tilde{I}_{out}(f_x,f_y)$ are the Fourier transforms of the input and output intensity distributions, respectively. The ATF allows to compare systems' response independently of the coherence of the illumination system. Thus, for the sake of simplicity while referring to correctly defined magnitudes, in this work we will refer to the *modulation transfer function* as $MTF=|\mathscr{H}_A|$, that is, the modulus of the ATF. In the case of rotational symmetric systems we will define $\mathscr{H}_A(u)$, being $u=\|(f_x,f_y)\|$.

3. Measurement methodology

Ideally, each angular profile of the SS pattern can be understood as a *rect* function repeated periodically. Therefore, this periodic structure could be represented as a Fourier series expansion

$$f(\theta)=\sum_{m=-\infty}^{\infty}C_m\cos\left(\frac{2\pi m\theta}{\Lambda}\right), \tag{2}$$

where the series coefficients are defined as $C_m=\frac{\sin\left(\frac{m\pi\alpha}{\Lambda}\right)}{m\pi}$, α is the angular width of the transmissive sectors of SS and Λ is the angular period.

From this definition, we can represent the intensity of the polar transformed SS pattern either in angular or spatial coordinates as

$$I^r_{SS}(\theta)=\sum_{m=-\infty}^{\infty}C_m\cos\left(\frac{2\pi m\theta}{\Lambda}\right)=\sum_{m=-\infty}^{\infty}C_m\cos\left(\frac{2\pi ml}{P(r)}\right)=I_{SS}(l,r), \tag{3}$$

where $P(r)=r\Lambda$ is the period of the fringes at each radius r and $l=\theta r$ is the arc length.

Applying the one dimensional Fourier transform along the angular variable θ we obtain

$$\tilde{I}^r_{SS}(\omega)=\sum_{m=-\infty}^{\infty}\frac{C_m}{2}\left[\delta\left(\omega-\frac{m}{\Lambda}\right)+\delta\left(\omega+\frac{m}{\Lambda}\right)\right], \tag{4}$$

#227116 - $15.00 USD Received 25 Nov 2014; revised 23 Jan 2015; accepted 27 Jan 2015; published 6 Apr 2015

where ω is the angular frequency variable. The angular position of the different diffraction orders $\omega_m = \frac{m}{\Lambda}$ is independent of the radius value. However, if we represent $\tilde{I}_{SS}$ as a function of the spatial frequency variable $u = \frac{\omega}{r}$, it becomes

$$\tilde{I}_{SS}(u,r) = \frac{1}{|r|} \sum_{m=-\infty}^{\infty} \frac{C_m}{2} \left[\delta\left(u - \frac{m}{\Lambda r}\right) + \delta\left(u + \frac{m}{\Lambda r}\right) \right], \tag{5}$$

where the position of the diffraction orders depend on the radius of the angular profile. Combining Eqs. (1) and (5) we obtain an expression to fulfill the values of $\mathscr{H}_A(u)$ in a range of frequencies given by the minimum and maximum reliable radius of the SS pattern for each m diffraction order:

$$\mathscr{H}_A\left(u = \frac{m}{\Lambda r}\right) = \frac{\tilde{I}^r_{SS}\left(\omega = \frac{m}{\Lambda}\right)}{\tilde{I}^r_{SS,ref}\left(\omega = \frac{m}{\Lambda}\right)}. \tag{6}$$

In practical terms, however, there are imperfections in the manufacturing of any SS, so that we cannot expect to have an ideal symmetric periodic structure. Therefore, the first task to do is to estimate the image of the experimental SS before degradations introduced by the optical system. The way to achieve this estimation is based on the notion that manufacturing $I^r_{SS,ref}$ should indeed produce a close to binary pattern, although not perfect. With this simple idea, $I^r_{SS,ref}$ is computed by thresholding I^r_{SS} in such a way that the minimum and maximum zones correspond to the mean of the minimum and maximum zones of the profile at the largest radius. We note that proceeding in this way produces a sharper edge, while preserving possible differences in width for clear and dark sections (as a drawback, it tends to produce too symmetric edges).

The workflow presented above is shown in Fig. 1. Figure 1(a) presents the experimentally acquired image of the SS, while Fig. 1(b) shows its representation in polar coordinates I^r_{SS}. The a posteriori estimation of $I^r_{SS,ref}$ is described in Figs. 1(c) and 1(d). Figure 1(c) corresponds to a cross-cut section through Fig. 1(b) at a given radius and angular range indicated by the red line, where the intensity values are shown as dots; note, also, the binary profile (straight lines) obtained after preprocessing. Figure 1(d) shows $I^r_{SS,ref}$, where we have kept the same red line mentioned previously. Finally, the 1D Fourier transform of the profile at largest radius of Fig. 1(d) is shown in Fig. 1(e). Note that Fourier series coefficients C_m for even order are not zero, as would be the case if clear and dark areas were equally spaced (as opposed to [13]), although the magnitude of the third order is clearly higher than the one of the second order, which turns out into a higher SNR. Consequently, in the following we will only consider odd order coefficients because of their greater SNR.

In Fig. 2(a) we show the profiles of the Fourier coefficients corresponding to $m = 1$ and $m = 3$ for both I^r_{SS} and $I^r_{SS,ref}$ at the corresponding spatial frequency $u = m/(\Lambda r)$ for each radius. If we calculate $|\mathscr{H}_A|$ for $m = 1$ and $m = 3$ (Fig. 2(b)), we observe that the curves overlap except for both the inverted peaks and the frequency range that correspond to the inner fringe ring of the SS pattern. The inverted peaks in the profiles correspond to the void rings of the SS pattern, while the inner ring is irregular enough to be considered unreliable. Since the position of the SS rings is a design parameter, it is easy to replace the values of the non-reliable ranges by interpolation, subsequently merging the $|\mathscr{H}_A|$ profiles at each m by averaging the overlapped range, leading to the final curve of the MTF (Fig. 2(c)).

To assure that the proximity to the Nyquist's limit is not influencing the measurement of each coefficient value of $|\mathscr{H}_A(u)|$, it is enough to select the proper angular resolution in the polar coordinates conversion such as the angular Nyquist's limit is far from the low orders.

4. Experimental results

We applied the proposed technique to calculate the MTF of one of the objective lens of the soft X-ray transmission microscope MISTRAL at ALBA synchrotron in Barcelone (Spain) [18].

#227116 - $15.00 USD Received 25 Nov 2014; revised 23 Jan 2015; accepted 27 Jan 2015; published 6 Apr 2015

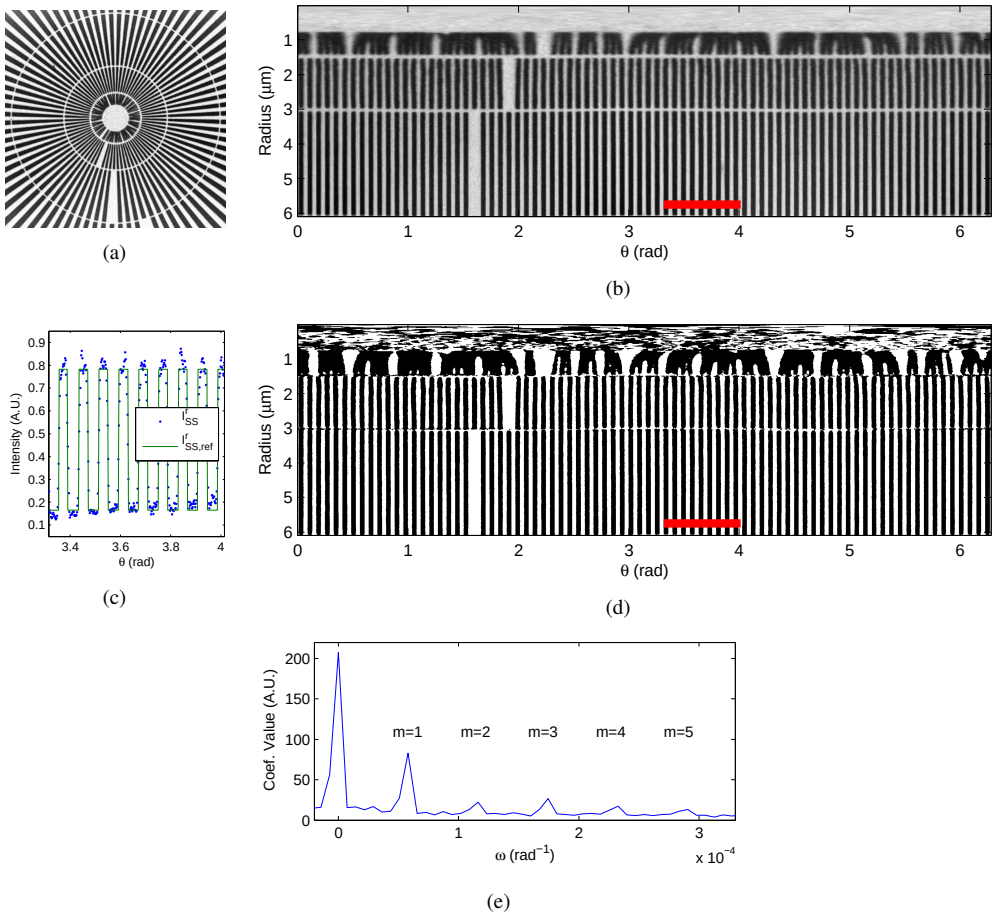

Fig. 1. (a) Siemens star test pattern; (b) Polar decomposition of (a); (c) $I^r_{SS,ref}$ profile calculated from the binarization of I^r_{SS} by thresholding, remarked by red lines in (d) and (b), respectively; (d) $I^r_{SS,ref}$ image in polar coordinates; (e) 1D Fourier transform of profile at largest radius from (d).

This is a Fresnel zone plate (FZP) characterized by an outermost zone width $dr_N = 25$ nm, 1500 zones and an illumination energy of 520 eV. The SS used in the experiments had 30 nm smallest features. Both the FZP and SS have been manufactured by Xradia Inc., now Zeiss. In Fig. 2(d) we show the calculated profiles of the MTF at different defocus distances. To compare, we have also calculated the theoretical profiles considering the numerical apertures of both the condenser and objective lenses ($NA_{condenser} = 0.029$ and $NA_{objective} = 0.0476$) as well as the one of the direct beam stop ($NA_{bs} = 0.0083$). We see in the case of the best focusing plane ($\Delta z = 0$ μm) that the cut-off frequency is around 0.022 nm^{-1}, slightly lower than the theoretical value of 0.032 nm^{-1} with lower contrast for the intermediate frequencies. However, when we observe the behavior against the defocus distances, we see that the experimental MTF width profiles decrease more slowly tan the theoretical ones. This can also be understood as the point spread function enlarges more slowly than in the theoretical case, being the experimental DOF greater than the expected one. We can also observe in the experimental profiles the valleys related to contrast inversion, as expected.

#227116 - $15.00 USD Received 25 Nov 2014; revised 23 Jan 2015; accepted 27 Jan 2015; published 6 Apr 2015

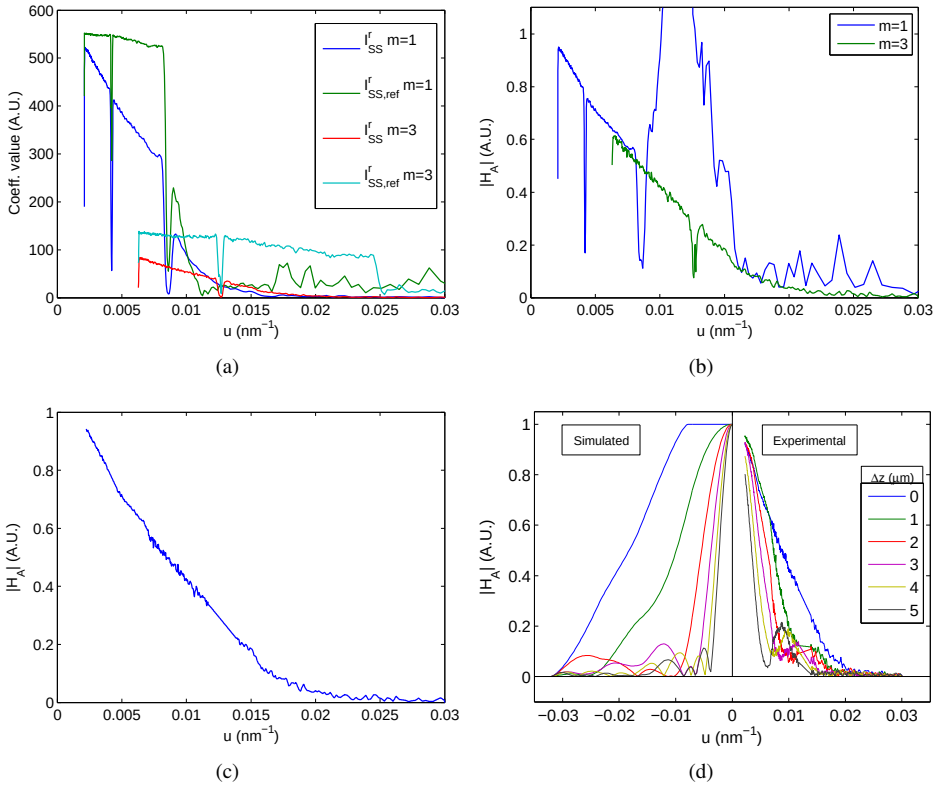

Fig. 2. (a) Plot of the Fourier coefficient values for 1^{st} and 3^{rd} diffraction orders for I^r_{SS} and $I^r_{SS,ref}$ against the corresponding spatial frequency; (b) $|\mathscr{H}_A|$ curves obtained from plots in (a); (c) Final experimental $|\mathscr{H}_A|$ curve obtained by combining curves in (b); (d) Comparison of simulated and measured MTF profiles for ZP with $dr_N = 25$ nm at different defocus distances.

5. Conclusions

We have introduced a method to calculate the MTF that is robust and can accommodate current manufacturing errors in the generation of test patterns, since the input reference pattern is estimated from the experimental image through a preprocessing step. We use a Siemens star pattern combining different Fourier orders in its polar decomposition, extending previous works that used a more limited frequency range. Finally, we applied the method to characterize the Mistral X-ray microscope MTF at different defoci, in order to evaluate the depth of field of the optics.

Acknowledgments

The authors would like to acknowledge economical support from the Comunidad de Madrid through grant CAM (S2010/BMD- 2305), the NSF through Grant 1114901, The Spanish Ministry of Economy and Competitiveness through Grants AIC-A-2011-0638, BIO2013-44647-R and BioStruct–X Project (contract number 283570). This work was partially funded by Instruct, part of the European Strategy Forum on Research Infrastructures (ESFRI) and supported by national member subscriptions.